Weldability of Intercritical Annealed Dual-Phase Steel with the Resistance Spot Welding Process

Low ductility in the nugget may impair resistance spot weldability

BY P. K. GHOSH, P. C. GUPTA, RAMAVTAR AND B. K. JHA

ABSTRACT. Optimum welding parameters for producing maximum joint strength in dual-phase steel are established, and the cause of weakening in the weldment is identified as tempering of martensite in the HAZ.

Introduction

Dual-phase steel is a new class of high-strength low-alloy steel having a microstructure of strong martensite and/or bainite colonies dispersed in a soft matrix of ferrite (Refs. 1, 2). These steels are produced either by continuous annealing/box annealing with the intercritical temperature range (Ref. 3) or by hot rolling (Ref. 4) low-alloy steels of various compositions. It is well known that these steels have a number of unique properties such as the absence of yield point, low yield/tensile strength ratio, high work hardening rate and usually a high, uniform and total elongation (Refs. 1, 5). The last two properties indicate very good formability which, coupled with its high tensile strength (Refs. 1, 6), makes it attractive for weight saving applications in the automobile industry for greater fuel economy (Refs. 1, 7). But the wide acceptance of this steel in the automobile industry is still not appreciable due to insufficient knowledge of its weldability using different welding processes. That is why in the past few years a considerable amount of effort has been made to understand the weldability of dual-phase steels under the flash welding (Refs. 8–11), shielded metal arc welding (Ref. 12) and resistance spot welding (Refs. 12–17) processes.

P. K. GHOSH and P. C. GUPTA are with the Welding Research Laboratory, Department of Mechanical and Industrial Engineering, University of Roorkee, India. RAMAVTAR and B. K. JHA are with RDCIS, Steel Authority of India Ltd., Ranchi, India.

For automotive applications, it is imperative for the material to possess good resistance spot weldability. The resistance spot weldability of steel to a great extent depends on the plate thickness, morphology of the base metal and its mechanical properties (Refs. 13, 15, 17). The morphology and properties of the base metal are governed by its chemical composition and the production process as discussed above. In most of the earlier works, the dual-phase steels produced by the hot rolling process and having a thickness in the range of 2.5 mm (0.1 in.) have been used to study weldability with the resistance spot welding process (Refs. 13–16). This is because of the popularity of comparatively thinner hot-rolled dual-phase steel in various industries due to economic reasons (Ref. 14). However, the production of dual-phase steels by the continuous annealing process has also been considered important by some workers (Refs. 18–20). This is possibly due to certain advantages, namely: 1) It requires less manganese (Ref. 21), 2) it gives less variation in mechanical properties in the products (Ref. 22), and 3) it produces a dual-phase microstructure of a well dispersed low-carbon martensite in a ferrite matrix. The high dislocation density at the interface with martensite facilitates the continuous yielding behavior of the steel (Refs. 23, 24). It has also been observed that the dual-phase steel developed by short-time intercritical annealing given to plates produced by hot rolling at high coiling temperature shows a higher resistance to autotempering during forming or fabrication (Ref. 25). As such, the use of intercritically annealed dual-phase steel in the automobile industry cannot be ignored (Ref. 26).

KEY WORDS

Resistance Spot Weld
Spot Welding
Steel Weldability
Dual-Phase Steel
Annealed Steel
Intercritical Anneal
Current Influence
Electrode Influence
Holding Time Effect
Fracture Behavior

A good spot welding practice requires optimization of the following parameters to achieve maximum strength of the joint (Refs. 17, 27):

1) An effective current to provide heat to the joint.
2) The weld time for current flow.
3) The electrode force that brings the components into intimate contact.
4) The holding time after welding for weld cooling.

In this work, an effort has been made to investigate the resistance spot weldability of 3.2-mm (0.125-in.) thick dual-phase steel sheet, produced by short-term intercritical annealing of hot rolled plates, by varying the welding parameters. The objective of this work is to identify the role of different welding parameters on the characteristics of the weldment and also to optimize the welding parameters to give maximum weld strength.

Experimental Procedure

Welding

The steel plates used in this study are 3.2 mm thick. They have a dual-phase microstructure, produced by intercritical annealing of hot-rolled plates for 8 min. at 1103 K followed by oil quenching. Chemical composition of the steel plates is given in Table 1. Samples of 38 or 50 × 125-mm (1.5 or 2 × 5-in.) heat-treated plates were resistance spot welded in a pneumatic phase shift AC spot welding machine of 184 kVA capacity.

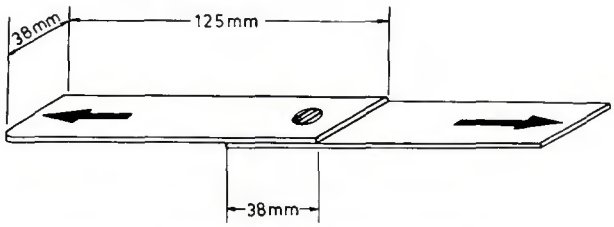

Fig. 1—Schematic diagram of tensile shear test specimen.

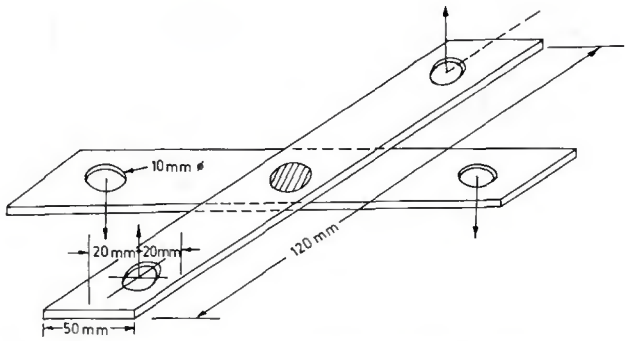

Fig. 2—Schematic diagram of cross-tensile test specimen.

Before welding, the surface of the plate was cleaned mechanically using Gr. 400 emery paper. Welding was performed with a water-cooled conical Cu-Cr alloy electrode having a diameter on its contact surface of about 9.0 mm (0.35 in.). The plates were welded linearly (Fig. 1) and crosswise (Fig. 2) to prepare specimens for tensile shear and cross-tensile tests. During welding, the various parameters, such as the effective current, electrode force, weld time and holding time were varied as shown in Table 2. The weld time and holding time are presented in a unit of 'cycles' where 100 cycles represent a time of 1 s. The effective current of welding was measured with the help of a troidal coil PECO weld current monitor (Type SM 12 A, Messer Griesheim) having a capacity of up to 200 kA. Other parameters, such as the electrode force, weld time and holding time were varied as desired by adjusting the controls available in the machine. The welding process is shown schematically in Fig. 3.

Tensile Test

The tensile properties of the base plate were determined by using standard (DIN 50120) flat tensile specimens. The tensile shear (Fig. 1) and cross tensile (Fig. 2) specimens were fabricated in close approximation to DIN 50124 and DIN 50164, respectively. All the tensile tests were carried out in a microprocessor-controlled servo hydraulic universal testing machine at a cross-head speed of 1 mm/min. During the tests, the ultimate test load was noted from the digital display in the machine and the deformation behavior (load vs. extension) was recorded using an x-y plotter.

Metallography

The welded specimens were cut transversely through the weld center. The transverse sections of base plate, as well as the weld specimens, were prepared by standard metallographic procedure and etched in 2% nital solution. The specimens were studied under optical and scanning electron microscopes.

The longitudinal section (weld surface) of the tensile shear test specimens fractured from the HAZ was prepared for metallographic observation under optical and scanning electron microscopes, where the location of the fracture and its morphology were studied. The typical nature of this type of failure as revealed in the longitudinal section of the specimen was recorded.

Microhardness Study

The microhardness measurements on the welded specimens and the base metal were carried out at a load of 981×10^{-3}N. During the microhardness study, the indentation was randomly made on the matrix without concern for the specific phases. However, in the case of the welded specimen, specific effort was made to indent the region identified as the weld center and at locations where a distinct change in microstructure was revealed. At a given effective current of 10.1 kA, the influence of varying welding time from 30 to 60 cycles on microhardness across the weld was reported.

The microhardness study was also carried out across the weld surface revealed in the longitudinal section of the tensile shear specimen fractured during testing.

Results

The mechanical properties of the base plate are shown in Table 3. During welding, expulsion was observed for certain parameters as shown in Table 2. The expulsion has been found to occur when the weld time is raised up to 60 cycles at an effective current of 10.1 kA and at a weld time of 30 cycles when the effective current is raised to 12.3 kA. It is also noted that at the effective current and weld time of 10.1 kA and 50 cycles, respectively, the welding at a low electrode force of below 500 kg (1100 lb) causes expulsion. During the tensile shear test, failure of the spot weld was found to occur at the interface as well as in the HAZ depending upon the welding parameters. However, in the cases where expulsion occurs, the weld invariably failed at the interface—Table 2.

Influence of Weld Time

For various values of effective current (9.2, 10.1 and 12.3 kA), the influence of variation in weld time on the ultimate tensile shear load-bearing capacity of the spot weld is shown in Fig. 4. The electrode force and holding time were kept constant at 565 kg (1243 lb) and 48 cycles, respectively. The figure shows that at a given effective current the increase in weld time to a certain extent increases the tensile shear strength of the weld, which is then followed by a decrease with a further increase in weld time. The critical

Fig. 3—Schematic diagram of the welding process.

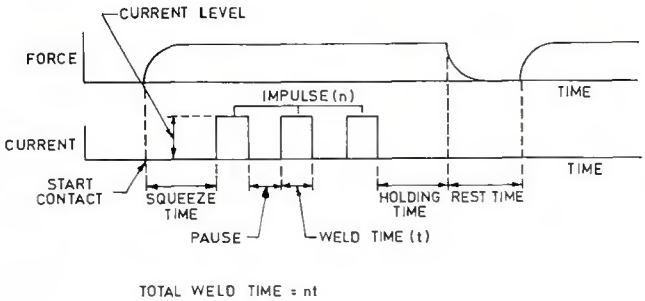

Table 1—Chemical Composition of the Base Plate (wt-%)

C	Mn	Si	Cr	Mo	S	P
0.068	1.02	0.92	0.48	0.3	0.028	0.02

weld time at which the weld shows maximum ultimate tensile shear strength decreases with an increase in effective current. Figure 4 also shows that the rate of increase in ultimate tensile shear strength with an increase in weld time is greater at a higher effective current than at a lower one. However, the maximum ultimate tensile shear load-bearing capacity of the weld (about 47.1 kN) was achieved when produced at the weld time of 50 cycles under an effective current of 10.1 kA.

The cross-tensile strength of a weld prepared at the effective current of 9.2 and 10.1 kA with varying welding time is shown in Table 4. The holding time and electrode force were kept constant at 48 cycles and 565 kg, respectively. The table shows that at an effective current of 9.2 kA the increase in weld time from 60 to 70 cycles decreases the ultimate cross-tensile strength of the weld. At an effective current of 10.1 kA, the increase in weld time from 45 to 50 cycles increases the ultimate cross-tensile strength of the weld from 18.84 to 20 kN.

Table 2—Scheme of the Welding Parameters and Their Performance

Squeeze Time (cycle)	Electrode Force (kg)	Effective Current (kA)	Weld Time (cycle)	Holding Time (cycle)	Remarks/Observations: During Welding	Remarks/Observations: During Tensile Shear Test
65	565	9.2	30	48	—	Interface failure
65	565	9.2	40	48	—	-do-[a]
65	565	9.2	50	48	—	HAZ failure
65	565	9.2	55	48	—	-do-
65	565	9.2	60	48	—	-do-
65	565	9.2	70	48	—	-do-
65	565	9.2	80	48	—	-do-
65	565	10.1	30	48	—	Interface failure
65	565	10.1	40	48	—	-do-
65	565	10.1	45	48	—	HAZ failure
65	565	10.1	50	48	—	-do-
65	565	10.1	60	48		Expulsion Interface failure
65	565	12.3	30	48	-do-	-do-
65	565	12.3	35	48	-do-	-do-
65	565	12.3	40	48	-do-	-do-
65	565	12.3	50	48	-do-	-do-
65	565	12.3	55	48	-do-	-do-
65	565	10.1	45	20	—	-do-
65	565	10.1	45	35	—	HAZ failure
65	565	10.1	45	60	—	-do-
65	375	10.1	50	48		Expulsion Interface failure
65	440	10.1	50	48	-do-	-do-
65	500	10.1	50	48	-do-	-do-
65	630	10.1	50	48	—	HAZ failure
65	702	10.1	50	48	—	Interface failure

(a) "do" means same as above.

Influence of Effective Current.

For various values of weld time kept at the level of 40, 50 and 60 cycles, the influence of increasing effective current from 9.2 to 12.3 kA on the ultimate tensile shear load-bearing capacity of the weld is shown in Fig. 5. The electrode force and holding time were kept constant at 565 kg and 48 cycles, respectively. The figure shows that at a given weld time of 40 cycles, the increase in effective current up to 12.3 kA increases the ultimate tensile shear strength of the weld. However, during welding at a weld time of 50 or 60 cycles, the increase in effective current from 9.2 to 10.1 kA enhances the ultimate tensile shear strength of the weld but it is followed by a decrease in strength with an increase to 12.3 kA.

Influence of Electrode Force

The influence of varying the electrode force from 375 to 702 kg (825 to 1544 lb) on the ultimate tensile shear load-bearing capacity of the weld is shown in Fig. 6. The effective current, weld time and holding time were kept constant at 10.1 kA, 50 and 48 cycles, respectively. The figure shows that the increase in electrode force from 375 to 565 kg enhances the tensile shear strength of the weld, but it decreases with a further increase in electrode force.

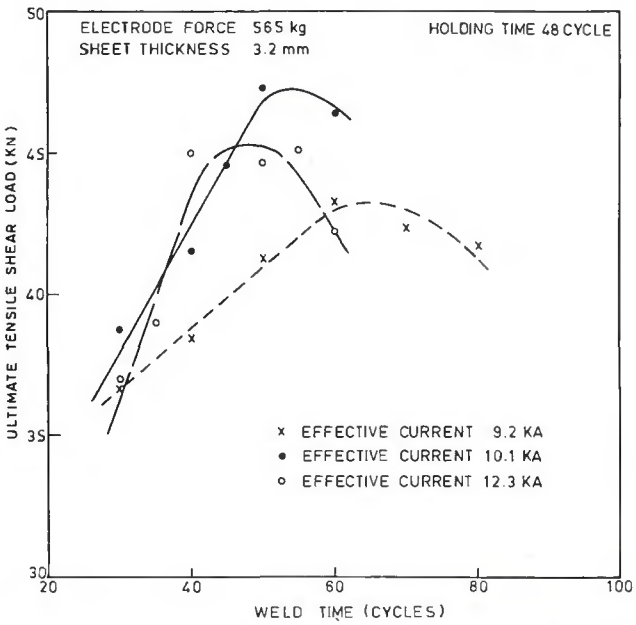

Fig. 4 — The influence of variation in welding time on the ultimate tensile shear load of the weldment at different currents.

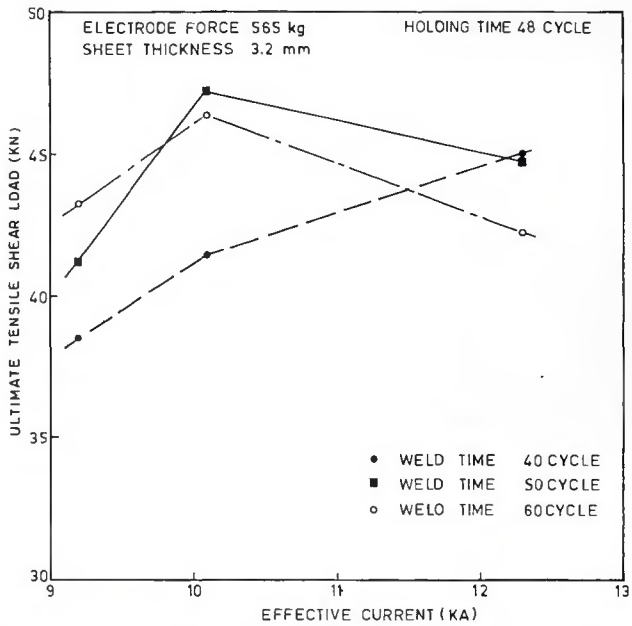

Fig. 5 — The influence of variation in effective current on the ultimate tensile shear load of the weldment at different weld times.

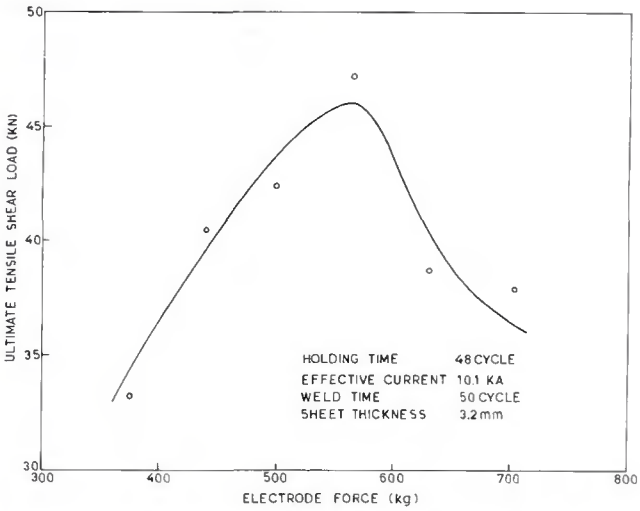

Fig. 6 – Influence of electrode force on the ultimate tensile shear load of the weldment.

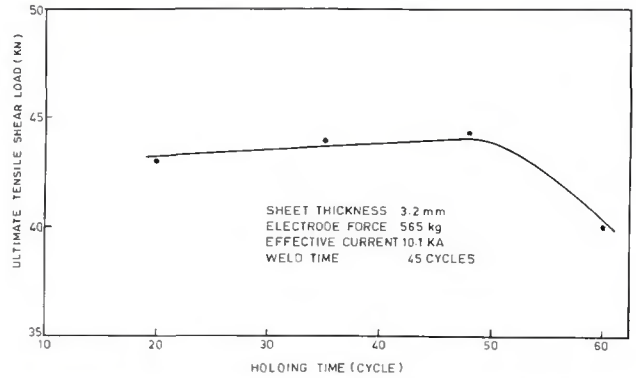

Fig. 7 – Influence of holding time on the ultimate tensile shear load of the weldment.

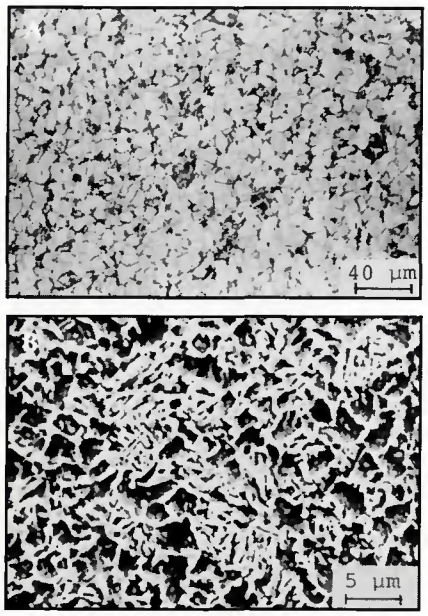

Fig. 8 – Microstructure of base metal. A – optical microscope; B – scanning electron microscope.

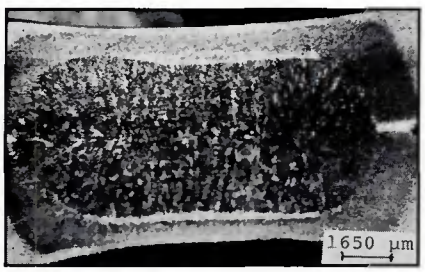

Fig. 9 – Typical macrograph of the spot weld.

Influence of Holding Time

The influence of holding time on the ultimate tensile shear load bearing capacity of the weld is shown in Fig. 7. It is shown in the figure that at a given effective current, weld time and electrode force of 10.1 kA, 45 cycles and 565 kg, respectively, the increase in holding time from 20 to 48 cycles shows a moderate enhancement in tensile shear strength, but that is followed by a significant decrease in strength with a further increase in holding time to 60 cycles.

Metallography

The microstructure of the base metal, as revealed under optical and scanning electron microscopes, shows a dual phase consisting of martensite colonies in a ferrite matrix – Fig. 8. A typical macrograph of the transverse section of the spot weld is shown in Fig. 9. The macrograph clearly shows the presence of an HAZ surrounding the weld nugget. The microstructure of the weld center and two different regions of the HAZ shows distinctly different morphologies as one goes away from the weld center – Figs. 10 and 11. The welds were produced at comparatively low and high weld times of 30 and 60 cycles, respectively, and the effective current, electrode force and holding time were kept constant at 10.1 kA, 565 kg and 48 cycles, respectively. The central region of the weld nugget was found to have bainite along with acicular proeutectoid ferrite of a Widemanstäten nature. It became coarser with the increase in weld time at a given effective current as shown in Figs. 10A and 11A. The microstructure of the HAZ (Figs. 10B and 11B) close to the weld nugget has a fine bainite and acicular ferrite structure; whereas, the other regions of the HAZ (Figs. 10C and 11C) away from the weld nugget are possibly tempered martensite. A comparison of HAZ microstructures as depicted in Figs. 10B and C and Figs. 11B and C reveals that the increase in weld time also coarsens the HAZ microstructure. The tempering of martensite observed at the outer region of the HAZ is revealed in Fig. 12.

Table 3—Mechanical Properties of the Base Plate

UTS (kg/mm²)	Elongation (%)	YS (kg/mm²)	Microhardness (VHN)
58.0	23	53.1	250

Microhardness Study

The microhardness behavior across welds made at weld times of 30, 45, 50 and 60 cycles is shown in Fig. 13. The ef-

Table 4—Cross-Tensile Strength of the Weldments Prepared with Different Welding Parameters

Squeeze Time (cycle)	Electrode Force (kg)	Effective Current (kA)	Weld Time (cycle)	Holding Time (cycle)	Ultimate Tensile Load (kN)	Remarks
65	565	9.2	60	48	18.38	HAZ failure
65	565	9.2	70	48	17.62	HAZ failure
65	565	10.1	45	48	18.84	HAZ failure
65	565	10.1	50	48	20.0	HAZ failure

fective current, electrode force and holding time are kept at 10.1 kA, 565 kg and 48 cycles, respectively. The figure shows that the center of the spot weld has a comparatively lower hardness than that of its surrounding matrix. This behavior is found to be more pronounced with a higher weld time of 60 cycles as compared to when a lower weld time is used. The hardness of the weld region also decreases with the increase in weld time. As one reaches the HAZ, the hardness goes down after showing an initial enhancement. It is also interesting to note that the weld prepared at the weld time of 45 cycles shows a valley of hardness at the HAZ, which vanishes with the increase in weld time.

Fracture Behavior

Fracture behavior of spot welds in a load vs. extension plot of the tensile shear test for welds prepared at various parameters is typically shown in Fig. 14. The curves depicted in the figure represent two different modes of fracture. One fractured at the weld and the other took place in the HAZ. In the case of the fracture in the weld, the curves drop immediately after reaching the ultimate load, but the fracture in the HAZ showed a smooth reduction in load over a range extending after the test was withdrawn. However, the curves do not show a typical yield point.

A typical failure in the HAZ and the location of initiation of fracture in this type of failure are shown in Figs. 15 and 16, respectively. The microhardness study carried out on the longitudinal section of the weld fractured in the HAZ, as shown in the macrograph presented in Fig. 16, has been depicted in Fig. 17. The figure shows that the fracture initiated from the region of the HAZ where there exists a valley of low hardness.

Discussions

The mechanical properties of a spot weld primarily depend on its nugget size, which is essentially governed by welding current and time; depth of electrode impression on the surface, which causes the thinning of the nugget; and the morphologies of the nugget and HAZ, which govern their strength and ductility. To achieve maximum strength, a spot weld must have a nugget volume large enough to provide, greater resistance to fracture as compared to the base metal or the HAZ, whichever is stronger. In the case of resistance spot welding of plain carbon steel, the HAZ does not become weaker than the base metal due to the formation of primarily martensite/bainite in it (Ref. 28). But during spot welding of dual-phase steel, there is always a possibility of forming a tempered martensite region at the

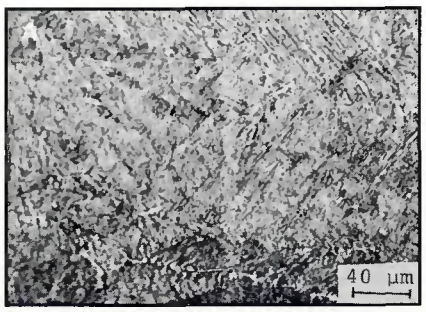

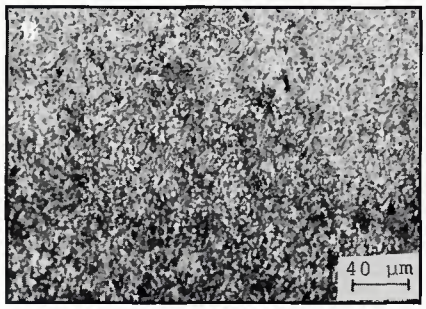

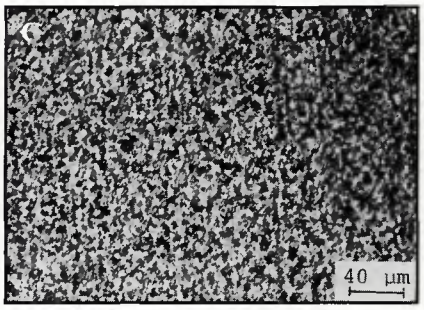

Fig. 10 — Microstructure of the weldment. A — weld center; B — HAZ; C — outer region of HAZ. Effective current = 10.1 kA, weld time = 30 cycles, electrode force = 565 kg and holding time = 48 cycles.

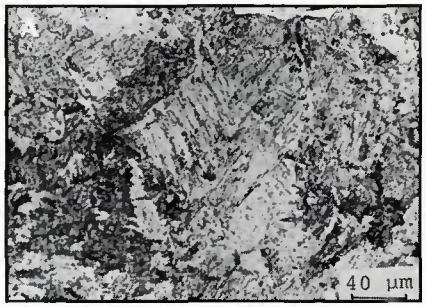

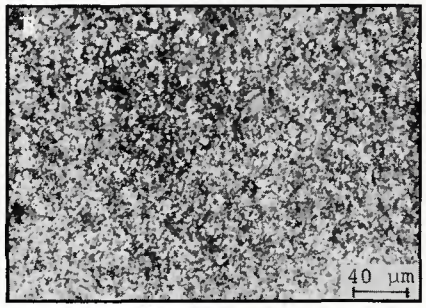

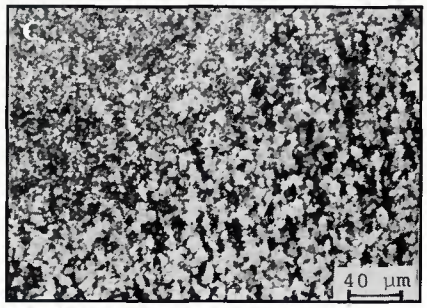

Fig. 11 — Microstructure of the weldment. A — weld center; B — HAZ; C — outer region of HAZ. Effective current = 10.1 KA, weld time = 60 cycles, electrode force = 565 kg and holding time = 48 cycles.

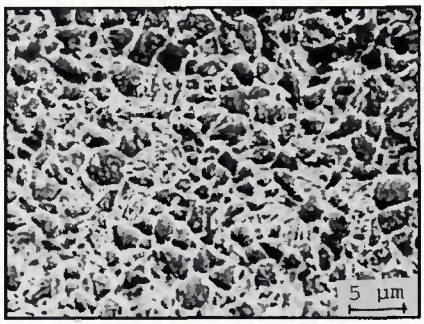

Fig. 12 — Scanning electron micrograph of the outer region of HAZ showing the presence of tempering of martensite.

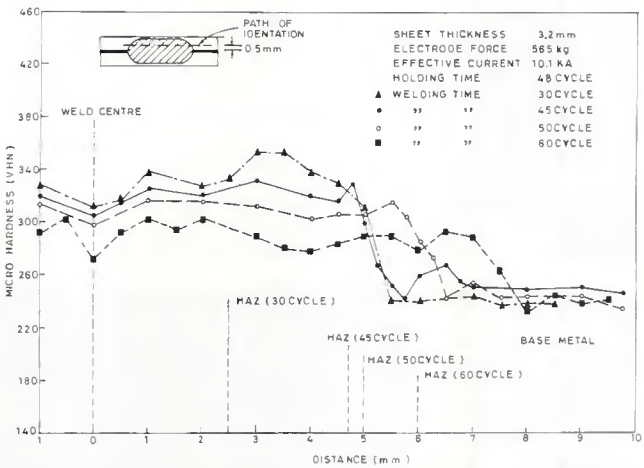

Fig. 13 — Microhardness across weld prepared at different weld times.

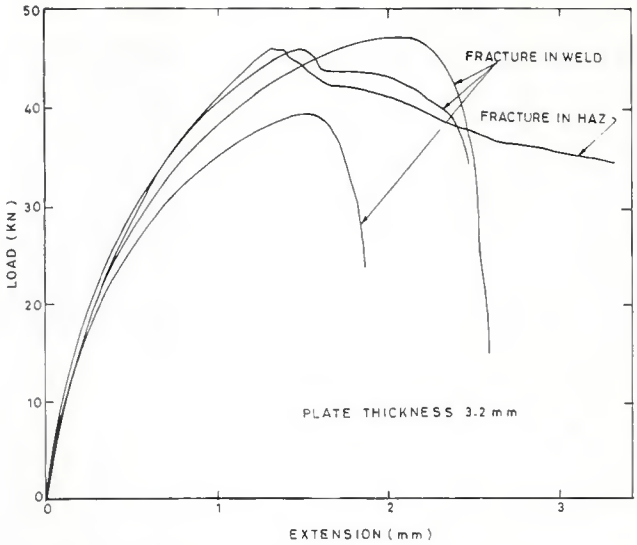

Fig. 14 — Load vs. extension plot of tensile shear test.

HAZ where the temperature is in the range of 600-650°C (1112-1202°F) (Refs. 17, 29). This region possesses a strength sometimes even lower than that of the base metal (Ref. 30). Thus, the strength of resistance spot welded dual-phase steel is competitive in nature between the load-bearing capacity of the nugget and the HAZ.

The morphology of the HAZ, which governs its strength and ductility, is primarily controlled by the weld thermal cycle and the morphology of the base metal. The thermal cycle is essentially governed by the energy input of the welding current and time. The reduction in energy input decreases the nugget size; whereas, an excessive energy input causes a coarsening in the HAZ microstructure. Moreover, at a given electrode force, the use of an excessive energy input, or at a given energy input the use of too low an electrode force, results in expulsion from the weld nugget, weakening it and causing a discontinuity. However, at a given energy input, the use of a high electrode force is also not advisable because it creates a deep impression in the weld region.

Influence of Weld Time at Different Currents

During resistance spot welding of 3.2-mm-thick, intercritical annealed, dual-phase steel at a comparatively low effective current of 9.2 kA, the weldments failed at the interface (nugget), due to a small nugget diameter (~ 8.0-8.5 mm), when the weld time was kept within 40 cycles. However, an increase in weld time to 50 cycles and above was found to weaken the HAZ, causing fracture in this region — Table 2. At a comparatively low welding current, there was a slow increase in nugget size with the increase in weld time accompanied by a weakening of the HAZ. This is possibly responsible for the restriction of the tensile shear strength of the joint at a low level — Fig. 4.

During welding at 10.1 kA, the weldment was found to fail at the interface when the weld time was kept within 40 cycles — Table 2. This happened when the nugget diameter was in the range of about 8.5-9.0 mm (0.33-0.35 in.), a diameter which cannot withstand a high tensile shear load. However, with an increase in weld time up to 50 cycles, the nugget diameter increased to about 11.75 mm (0.46 in.) with the increase in weld time beyond 45 cycles, the increase in nugget diameter beyond that of the electrode may have occurred due to excessive conduction heating of the metal around the electrode. The weld joint prepared at a weld time of 50 cycles achieved its maximum strength as reflected in its ultimate tensile load-bearing capacity — Fig. 4. But it was observed (Table 2) that in the tensile shear test the joint prepared at 10.1 kA started rupturing in the HAZ when the weld time reached a level of 45 cycles. The increase in weld time weakened the HAZ, as depicted in the microhardness study across the weld — Fig. 13. This was due to the coarsened HAZ morphology as evident in the micrographs presented in Figs. 10B and C and 11B and C where the weld time was 30 and 60 cycles, respectively. However, the relatively higher hardness observed in the HAZ adjacent to the weld nugget may have been caused by some favorable metallurgical transformation in this region, possibly due to comparatively faster cooling under the influence of a self-cooled electrode. It was also observed that the fracture in the HAZ always takes place from its outer region, as typically shown in Figs. 15 and 16. The microhardness study carried out across the weld that ruptured in the HAZ (Fig. 17) showed that the fracture took place in the weakest region in the HAZ, which is sometimes softer than the base metal (Figs. 13 and 17), due to tempering of martensite (Fig. 12) in this region. During welding at a weld time of 60 cycles, significant coarsening of the tempered martensite region (Fig. 11C) may have caused an early failure of this region, resulting in reduced strength (Fig. 4) in the weld joint.

The increase in current to 12.3 kA

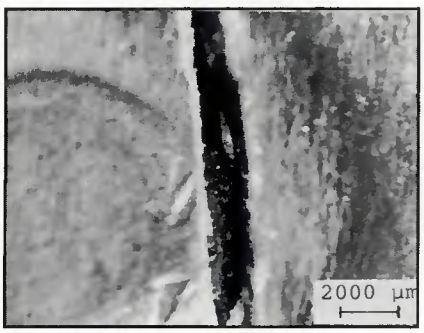

Fig. 15 — Typical nature of failure from the HAZ.

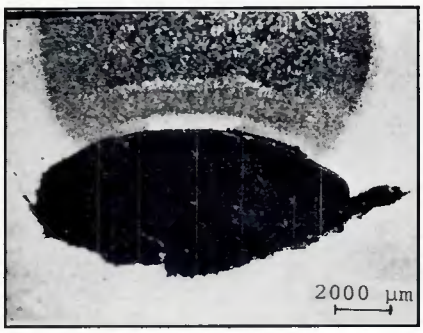

Fig. 16 — Macrograph showing the nature of fracture at the outer region of the HAZ.

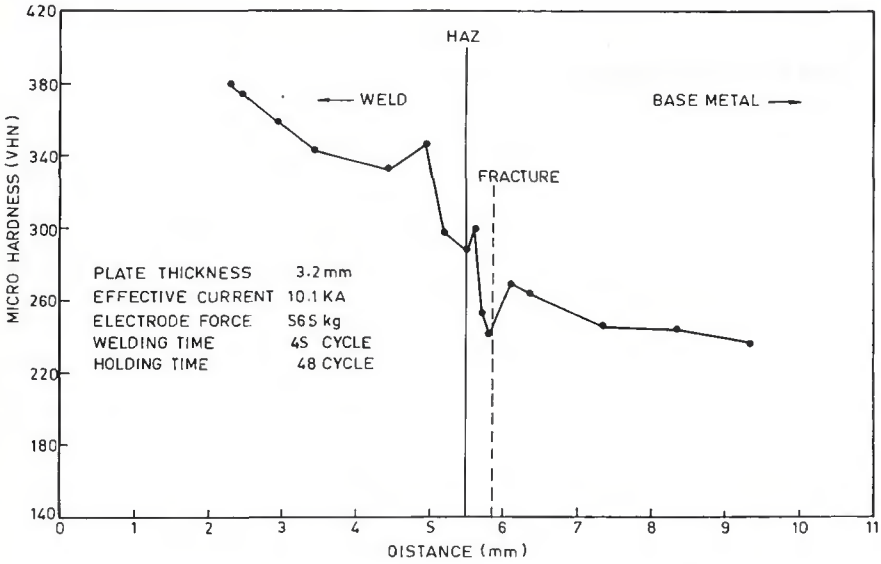

Fig. 17 — Microhardness across the longitudinal section of the weld fractured at the HAZ, as shown in Fig. 16.

resulted in expulsion, even at a low weld time of 30 cycles, and weakened the weld nugget, which always caused a failure the same as shown in Table 2. Thus, at this level of effective current, though the nugget size was increased with the enhancement of weld time, the strength of the weldment could not be raised to a maximum — Fig. 4.

It is interesting to note in the above discussion that during welding at the effective current in the range of 9.2–10.1 kA, the weldment started fracturing at the HAZ when the weld time was kept in the range of 45–50 cycles (Table 2). This behavior infers that during resistance spot welding of the present type of dual-phase steel (3.2 mm thick), keeping the weld time at the level of 45–50 cycles is sufficient for a significant weakening of the HAZ by tempering of martensite. The results depicted in Fig. 5 further confirm the phenomenon observed above, where it is clearly seen that good strength of the weldment is obtained when the workable range of effective current does not exceed 10.1 kA, and the weld time does not exceed 50 cycles. The cross-tensile strength of the weldments prepared at 9.2 kA and 10.1 kA presented in Table 4 also shows an agreement with the observations of the tensile shear strength results (Fig. 4), where the tensile load-bearing capacity of the weldments was found to be maximum at 60 and 50 cycles, respectively. The fracture was found to occur at the HAZ — Table 4.

Influence of Electrode Force

At a low value of electrode force (500 kg), only a few contact bridges are established, resulting in a high local current density and a melting/fusion at some spots, which causes an expulsion during welding — Table 2. However, with the increase in electrode force, more contact bridges are established, resulting in uniform heating and melting of larger areas. This has minimized expulsion during welding and improved the strength of the weldments, displaying a maximum strength when the electrode force reached 565 kg (Fig. 6), a point at which no expulsion was observed — Table 2. But a further increase in electrode force increased the depth of electrode impression considerably and reduced the strength of the weldment (Fig. 6) significantly due to a thinning of the joint region.

Influence of Holding Time

During holding time, the weld joint cools down under electrode force, which possibly affects the behavior of the phase transformation at the weld nugget. This may have manipulated the strength of the weldment — Fig. 7. However, to understand this behavior, a further study has to be carried out in detail.

Conclusions

In this class of steel, the welding parameters of effective current and weld time primarily govern the thermal cycle of the weldment and control the weld strength to a great extent due to the tempering of martensite in the outer region of the HAZ. The tempering of martensite may have improved the overall ductility of the weld, but its response to early local necking under tensile loading possibly impairs the strength of the weldment. The workable effective current that produces no expulsion, but causes a reduction in joint strength, is approximately 10.1 kA. The increase in weld time beyond about 45–50 cycles causes a significant weakening in the HAZ due to the tempering of martensite at its outer region, which acts as a susceptible zone of rupture. The electrode force and holding time also were found to influence the joint strength. The maximum joint strength was achieved when the welding parameters of effective current weld time, electrode force and holding time are kept at 10.1 kA, 50 cycles, 565 kg and 48 cycles, respectively. However, it is observed that the resistance spot weldability of this steel is relatively poor as revealed by its ductility. This may be attributable to the high carbon equivalent and high sulfur content of the steel.

References

1. Rashid, M. S. 1976. A unique high-strength sheet steel with superior formability. *SAE Trans.* 85:938.

2. Davies, R. G. 1978. Influence of martensite composition and content on the properties of dual-phase steel. *Met. Trans.* 9A:671.

3. Matsuoka, T., and Zamomori, K. 1975. Metallurgical aspects in cold-rolled high-strength steel sheets. *Met. Trans.*, 6A:1613.

4. Coldren, A. P., and Tither, G. 1978. Development of a Mn-Si-Cr-Mo as rolled dual-phase steel. *J. Metals*, 30(4):6.

5. Ohashi, N., Takahashi, I., and Hashiguchi, K. Processing techniques and formability of age hardenable, low-yield, high-tensile-strength cold-rolled sheet steels. *Trans. ISI Japan* 18:321.

6. Hayami, S., and Furukawa T. 1975. A family of high-strength cold-rolled steels. *Proc. Conf. Microalloying 75*, 2A, Vanitec, London, England, p. 78.

7. Rashid, M. S., and Lawrence, G. D. 1978. Wheel weight reduction with GM980X steel. *SAE Trans.* 87:552.

8. Yamauchi, N., Taka, T., Kunishige, K., and Nagao, N. 1982. Softening behavior in heat-affected zone of flash butt welded hot-rolled dual-phase steel. *Trans. ISI Japan* 22(4):107.

9. Jha, B. K., Mishra, N.S., and Ramaswamy, V. 1983. An investigation into flash butt weldability of hot-rolled dual-phase steel. *Steel India*

6(2):114.

10. Ghosh, P. K., Gupta, P. C., Ramavtar, and Jha, B. K. 1988. Weldability of dual-phase steel under flash butt welding process. *Proc. Int. Conf., Welding Technology in Developing Countries Present Status and Future Needs.* Univ. of Roorke, India, II-53.

11. Jha, B. K., Ramavtar, Dwivedi, V. S., and Ramaswamy, V. 1988. Flash butt welding of dual-phase steel—a case study. *Proc. Int. Conf. Welding Technology in Developing Countries—Present Status and Future Needs.* Univ. of Roorkee, India, III-199.

12. Gupta, P. C., and Ghosh, P. K. 1988. Weldability of dual-phase steel produced by Steel Authority of India Ltd. Project Report, Welding Research Laboratory, MIED, Univ. of Roorkee, Roorkee, India.

13. Pollard, B., and Goodenov, R. H. 1979. Spot weldability of dual-phase steel. SAE tech. paper series, 790006.

14. Bryhan, A. J. 1977. The effect of carbon content on the resistance spot weldability of as-rolled dual-phase HSLA steels. Climax Molybdenum, Michigan, R&D Report, L-176-185.

15. Pollard, B. 1974. Spot welding characteristics of HSLA steel for automative applications. *Welding Journal* 53(8):348.

16. Sawhill, J. M., and Furr, S. T. 1981. Spot weldability tests for high-strength steels. SAE tech. paper 810352.

17. Ghosh, P. K., Gupta, P. C., Ramavtar, and Jha, B. K. 1990. Resistance spot weldability of comparatively thick C-Mn-Cr-Mo dual-phase steel sheet. *ISIJ Int.* 30(3):233.

18. Hayami, S., and Furukawa, T. 1975. A family of high-strength cold-rolled steels. *Proc. Conf. Microalloying 75,* 2A, Washington D.C., p. 78.

19. Hayami, S., Furukawa, T., Gondoh, H., and Takechi, H. 1979. Recent developments in formable hot- and cold-rolled HSLA including dual-phase sheet steels. *Formable HSLA and Dual Phase Steels,* ed., A. T. Davenport, AIME, New York, N.Y., p. 167.

20. Deleon, Y., Hochon, B., and Jussiaume, A. 1984. User demands and experience of continuously annealed steels for automative applications. *Scandinavian Met.,* 13(6):352.

21. Okamoto, A., and Takahashi, M. 1981. Control of strength and R- value in box-annealed dual-phase steel sheet. *Proc. Conf., Fundamentals of Dual Phase Steels.* ed., R. A. Kot and B. L. Bramfitt, AIME; Chicago, Ill., p. 427.

22. Kato T., Hashiguchi, K., Takahashi, I., Irie, T. and Ohashi, N. Development of hot-rolled dual-phase steel sheet. *Proc. Conf. Fundamentals and Dual Phase Steels, ed.,* R.A. Kot and B. L. Bramfitt, AIME; Chicago, Ill., p. 199.

23. Koo, J. Y., Raghvan, M., and Thomas, G. 1980. Compositional analysis of dual-phase steels by transmission electron microscopy. *Met. Trans.,* 11A, p. 351.

24. Mathy, H., Messien, P., and Greday, T. 1980. Aspects des performances potentialities des aciers multiphase power toles de diverses epaisseurs. *Revue de Metallurgie-CIT,* 421, p. 421.

25. Furukawa, T., and Tanino, M. 1981. Structure formation and mechanical properties. *Proc. Conf., Fundamentals of Dual Phase Steels,* ed., R. A. Kot and B. L. Bramfitt, AIME, Chicago, Ill., p. 221.

26. Sawhill, J. M. 1984. Spot weldability of high-strength sheet steels, continuously heat treated and batch annealed. *Proc. Sheet Metal Welding Conf.,* Detroit, Mich., p. 15.

27. Sawhill, J. M. Jr., Watanabe, H., and Mitchell, J. W. 1977. Spot weldability of Mn-Mo-Cb, V-N and SAE 1008 steels. *Welding Journal* 56(7):217-s.

28. Gupta, P. C., Raina, C. L., and Singh, B. K. 1988. Effect of welding parameters on strength of steel spot welds. *Procd. Int. Conf. Weld Tech. in Developing Countries—Present Status and Future Needs,* Univ. of Roorkee, India, I-135.

29. Ghosh, P. K. 1990. Thermal cycle and microstructure of heat-affected zone (HAZ) of flash butt welded Mn-Cr-Mo dual-phase steel. *ISIJ Int.,* 30(4):317.

30. Ghosh, P. K., Dorn, L. Influence of weld thermal cycle on the properties of flash butt welded dual-phase steel. Submitted to *Schweissen Schneiden.*